

OPEN

Urea assisted ceria nanocubes for efficient removal of malachite green organic dye from aqueous system

Thupakula Venkata Madhukar Sreekanth¹, Patnamsetty Chidanandha Nagajyothi¹, Gutturu Rajasekhara Reddy², Jaesool Shim¹ & Kisoo Yoo¹

This study describes a simple, high-yield, rapid, and inexpensive route for the synthesis of cubic shape-like cerium oxide nanocubes (CeO₂ NCs) using different urea concentrations (0.5, 1.0, and 2.0 g) by the hydrothermal method. The synthesized nanocubes (NCs) are labeled as CeO₂ NCs-0.5, CeO₂ NCs-1.0, and CeO₂ NCs-2.0, corresponding to 0.5, 1.0, and 2.0 g of urea, respectively. The synthesized NCs were characterized by FT-IR, UV-visible, XRD, XPS, SEM and HR-TEM analysis. The synthesized NCs were cubic in shape with average sizes of 12, 12, and 13 nm for the CeO₂ NCs-0.5, CeO₂ NCs-1.0, and CeO₂ NCs-2.0, respectively, obtained by the XRD analysis. The catalytic activity of the CeO₂ NCs was studied for the purpose of obtaining the reduction of malachite green (MG) in the presence of sodium borohydride (NaBH₄) at room temperature.

Environmental pollution is one of the most serious problems facing human beings and other life forms due to the increasing population, industrialization, and urbanization¹. Dyes are major pollutants that are released from textile industrial effluent². Malachite green (MG, including aniline green; basic green 4; diamond green B; and victoria green B) is a water-soluble cationic dye that is available in two forms malachite green chloride (C₂₃H₂₅ClN₂) and malachite green oxalate (C₅₂H₅₄N₄O₁₂) (Table 1). It is used as an industrial dye for the dyeing of leather, wool, silk, cotton, jute, paper and the manufacturing of printing inks and paints³. The extensive usage of MG dye has caused several health problems, including significant effects on the immune and reproductive systems⁴. MG also has the potential to cause genotoxic and carcinogenic effects and is extremely cytotoxic to mammalian cells⁵, and hence the suitable treatment of wastewater containing MG dye is highly necessary. Several methods have been developed, such as physical, chemical, biological, and photocatalytic degradation methods for the treatment of industrial effluent^{3,6–9}. The physical and chemical methods include adsorption¹⁰, ion-exchange¹¹, irradiation¹², oxidation processing¹³, chemical precipitation¹⁴, photolysis¹⁵, coagulation/flocculation¹⁶, electrochemical treatment¹⁷, ozonisation¹⁸, photo-Fenton degradation^{19,20}, reduction and oxidation²¹. The biological methods include fungal degradation²², bacterial degradation²³, and aerobic and anaerobic degradation²⁴. However, these methods are generally expensive, are unable to completely remove the dye, and produce high sludge and by-products that cause secondary pollution²⁵. In recent years photocatalytic degradation of organic dyes has been used effectively, but this process is slow and energy-consuming. Compared with photocatalytic activity, a catalytic reduction is a relatively fast process without high energy requirements²⁶.

Ce is a rare earth element with a wide bandgap (~3.2 eV), lanthanide series, and exists as a free metal or oscillates between in the Ce³⁺ and Ce⁴⁺ oxidation states²⁷. CeO₂ NCs, also known as nanoceria, have been widely used in catalysis, fast-ion conductors, UV blockers, energy storage, and optical sensors due to its excellent physical and chemical properties^{28–31}.

CeO₂ is an effective catalyst for the removal of organic dyes from effluents because ceria also hops between Ce³⁺ and Ce⁴⁺ valence states containing oxygen vacancies that allow NCs to act as regenerative catalysts³². Various methods have been reported in the literature for the synthesis of ceria^{33–37}, including sol-gel³⁸, microwave combustion³⁹, flame spray pyrolysis⁴⁰, solvothermal⁴¹, microemulsion⁴², spray drying system⁴³, hydrothermal⁴⁴,

¹School of Mechanical Engineering, Yeungnam University, Gyeongsan, 38541, Republic of Korea. ²Department of Instrumentation, Sri Venkateswara University, Tirupati, 517 502, India. Correspondence and requests for materials should be addressed to K.Y. (email: kisoooyoo@yu.ac.kr)

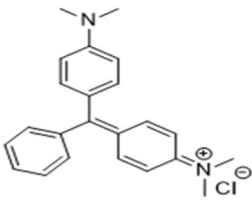
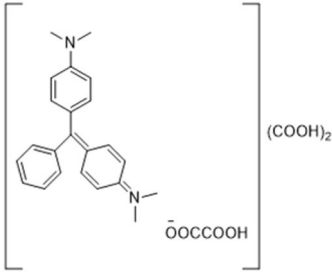
Properties	Malachite green chloride	Malachite green oxalate
Molecular formula	C ₂₃ H ₂₅ ClN ₂	C ₅₂ H ₅₄ N ₄ O ₁₂
Molecular weight	364.911 g/mol	927.00 g/mol
Max. wavelength (λ_{\max})	618 nm	618 nm
Structure		

Table 1. Chemical properties of malachite green (MG) dye.

and thermal decomposition⁴⁵. Among these, the hydrothermal method is simple, which can produce high product yields⁴⁶.

In this study we synthesized CeO₂ NCs using urea (CH₄N₂O), as capping and reducing agent, urea was also known as carbamide and it is easily soluble in water. It has been used as a nitrogen source for the synthesis of environmentally benign nanoparticles. It has been widely used in many industries such as in agriculture, plastic, drug, soap, and detergent industries. However, excess concentrations urea in soil or in water causes to soil acidification and eutrophication and toxic effects to aquatic organisms, animals and humans^{47,48}. The ceria nanocubes (CeO₂ NCs) were synthesized via the one-pot hydrothermal method using different concentrations of urea. The CeO₂ NCs are applied as a catalyst for the degradation of MG in the presence of NaBH₄ in an aqueous medium using UV-visible spectroscopy.

Materials and Methods

Materials. Analytical grade cerium nitrate hexahydrate and urea were purchased from Alfa-Aesar, South Korea and used directly. Malachite green dye was obtained from Daejung Chemicals, South Korea. Deionized (DI) water was used throughout the study for the synthesis of CeO₂ NCs and dye degradation studies.

Synthesis of ceria nanocubes. Cerium nitrate hexahydrate, 0.01 M was prepared at a volume of 70 mL in DI water. Different quantities of urea (0.5, 1.0 and 2.0 g) were added and stirred until dissolved. This reaction mixture was transferred to an autoclave at a temperature of 180 °C for 6 h. The reaction solution was naturally cooled down to room temperature. The reaction mixture was carefully collected by centrifuge and washed with DI and ethanol to remove the unreacted substance, before drying at 80 °C overnight. This was later calcined at 400 °C for 4 h and for comparison we prepared ceria without urea (CeO₂ NCs-0.0).

Characterization. The crystallinity was measured by an X-ray diffractometer (PANalytical X-Pert PRO, USA) using a Cu K α source ($\lambda = 1.5405 \text{ \AA}$). FT-IR (Perkin-Elmer, Bruker) was used to identify the vibrational modes by an ATR mode. The morphology of the samples was investigated by scanning electron microscopy (SEM-4800, Hitachi) and high-resolution transmission electron microscopy (TEM, Titan G2 ChemiSTM Cs Probe) with a 200 kV field emission gun in high brightness Schottky mode FEG (X-FEG). UV-visible absorption was measured on a Neogen (NEO-D3117). The elemental composition was quantitatively compared using an X-ray photoelectron spectrometer (K-alpha, Thermo Scientific, USA) with Al K α radiation (1486.6 eV).

Catalytic activity. The synthesized samples were used to check the catalytic ability using the MG dye. For the catalytic reactions, 2.5 mL of the MG dye, 25 μ L of well-dispersed CeO₂ NCs (2 mg/mL) and 0.2 mL of (0.2 M) freshly prepared NaBH₄ were added to all the samples. The degradation efficiency was monitored by UV-visible spectroscopy (Neogen, NEO-D3117). The degradation efficiency was calculated as a function of time for C_o/C_t and $\ln C_o/C_t$, where C_o is initial concentration and C_t is the final concentration of the MG dye. Blank control experiments were performed without catalyst (MG + NaBH₄) or NaBH₄ (MG + CeO₂ NCs) to study the catalyst efficiency.

Results and Discussion

Characterization. The UV-visible absorbance spectra of the ceria nanocubes are shown in Fig. 1. The synthesized ceria nanocubes exhibited broad absorption peaks below 400 nm. Couple of broad absorption peaks were observed at wavelengths 208 and 311 nm (CeO₂ NCs-0.5); 209 and 310 nm (CeO₂ NCs-1.0); and 209 and 314 nm (CeO₂ NCs-2.0). These peaks correspond to the characteristic absorption peaks of Ce³⁺ and Ce⁴⁺ of the CeO₂ NCs. These results are similar to those obtained by Nurhasanah⁴⁹ *et al.* who observed absorption peaks at 207 and 303 nm for CeO₂ NCs (9 nm, precipitation method).

Fig. 2 shows the FT-IR spectra of the as-synthesized urea-based ceria nanocubes (CeO₂ NCs-0.5, CeO₂ NCs-1.0, and CeO₂ NCs-2.0). The features near 1540 and 1630 cm⁻¹ related to (ν C=O) and (N-H stretching) bond stretch^{50,51}. The remaining observed peaks are as follows: near 3362 cm⁻¹ (O-H stretching vibrations)⁵²; near 2980 cm⁻¹ (asymmetric C-H stretching)⁵³; sharp band near 1340 cm⁻¹ (N-O stretch due to the presence of

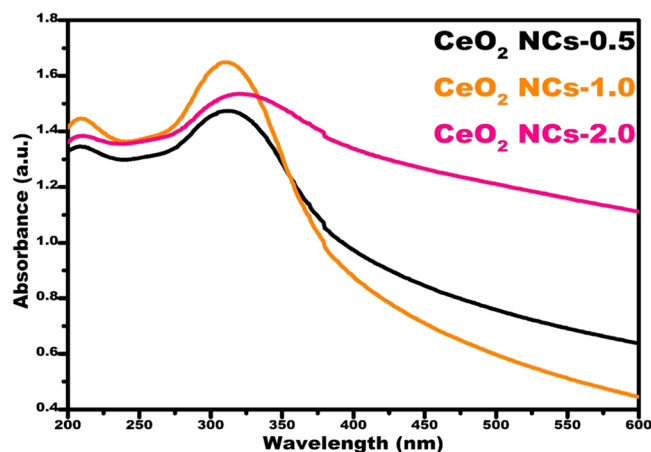


Figure 1. UV-visible spectra of the cerium oxide nanocubes (CeO_2 NCs) as a function of urea concentration.

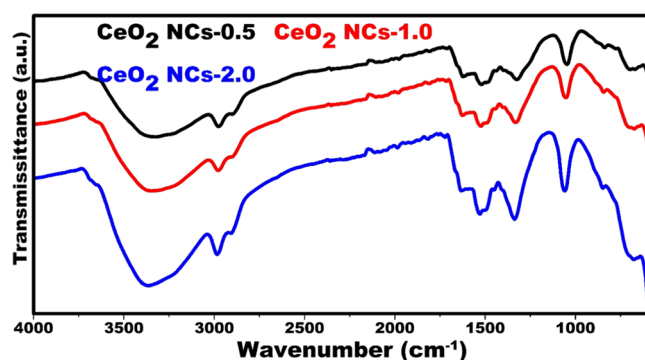


Figure 2. FT-TR spectra of cerium oxide nanocubes (CeO_2 NCs) as a function of urea concentrations.

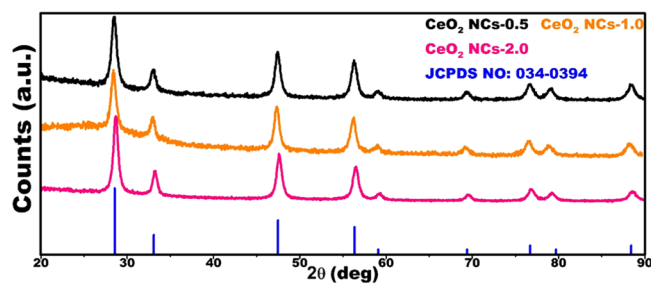


Figure 3. XRD spectra of the cerium oxide nanocubes (CeO_2 NCs) as a function of urea concentrations.

nitrate)⁵⁴; 1071 cm^{-1} (C-O stretching vibration)⁵⁵; 850 cm^{-1} (formed by CeO_2 , which is typical peak of the Ce-O stretching vibrations)⁵⁶; and below 700 cm^{-1} (O-Ce-O stretching vibrations)⁵⁷.

Fig. 3 shows the XRD patterns of urea-based 0.5, 1.0 and 2.0 CeO_2 NCs. The XRD revealed sharp peaks which located at $2\theta = 28.5^\circ, 32.9^\circ, 47.5^\circ, 56.3^\circ, 59.0^\circ, 69.3^\circ, 76.7^\circ, 78.8^\circ,$ and 88.4° , are corresponding to (111), (200), (220), (311), (222), (400), (331), (420) and (422) planes, respectively. No extra peaks were observed, which supported the assumption that urea-based NCs are pure with cubic fluorite structure (JCPDC: 034–0394), similar peaks were also observed in CeO_2 NCs-0.0 and results are shown in Fig. S1. The average mean grain size (MGS) of the NCs was calculated by the Debye-Scherrer equation as follows^{58,59}:

$$\text{MGS} = 0.94\lambda / \beta \cos\theta \quad (1)$$

where β is the broadening in the full-width at half maximum (FWHM), λ is the X-ray wavelength (1.5406 \AA), and θ is the Bragg diffraction angle. The microstrain, ϵ , of the NCs is evaluated by

$$\epsilon = (\beta \cos\theta) / 4 \quad (2)$$

Sample	Peak degree (°)	Diffraction plane	Mean grain size (nm)	Dislocation density ($\delta \text{ m}^{-2}$)	Microstrain (ϵ)	Lattice strain (LS)
CeO ₂ NCs-0.5	28.5	111	12	0.006	0.003	0.011
CeO ₂ NCs-1.0	28.5	111	12	0.005	0.003	0.011
CeO ₂ NCs-2.0	28.5	111	13	0.005	0.003	0.010
CeO ₂ NCs-0.0	28.3	111	31	0.0009	0.001	0.004

Table 2. Calculated XRD parameters of the urea assisted CeO₂ NCs.

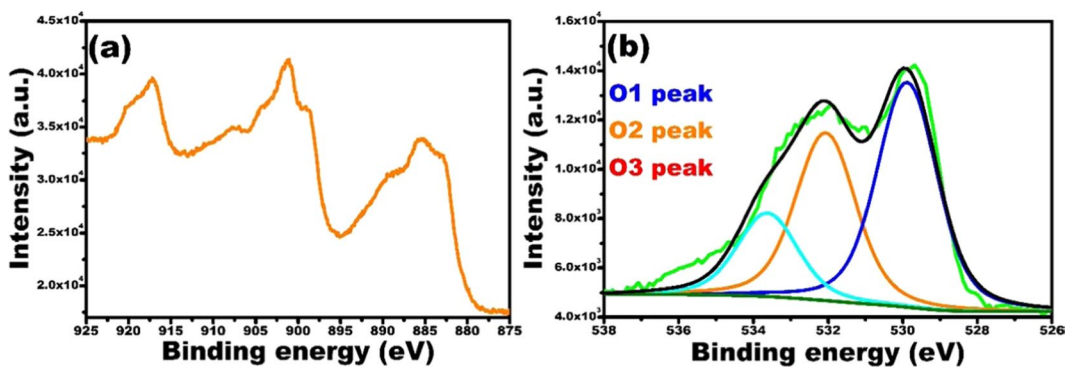


Figure 4. XPS analysis of the CeO₂ NCs-0.5; high-resolution spectra of cerium (Ce 3d (a)) and oxygen (O 1s (b)).

The dislocation density δ , of the NCs is defined as the length of dislocations lines per unit volume and given by

$$\delta = 1/(MGS)^2 \quad (3)$$

The lattice strain (LS) of the NCs was calculated using the following relation^{60,61}.

$$LS = \beta/4 \tan \theta \quad (4)$$

From Table 2, the MGS increased with the increasing urea concentration, for CeO₂ NCs-0.5 and CeO₂ NCs-1.0 were showing similar value (12 nm), and for CeO₂ NCs-2.0 showing slightly bigger size (13 nm), whereas CeO₂ NCs-0.0 showing much higher than (31 nm) urea mediated CeO₂ NCs, this MGS analysis clearly indicating the urea was acted as capping and reducing agent to control the size of the NCs, meanwhile, the dislocation density decreased with increasing urea concentration, but for higher concentrations (CeO₂ NCs-1.0 and CeO₂ NCs-2.0) dislocation density was constant, in CeO₂ NCs-0.0 too low than the urea mediated CeO₂ NCs. The microstrain was constant with increasing urea concentration but without urea CeO₂ NCs showing lower than other CeO₂ NCs, however, lattice strain (LS) was constant for the first two concentrations (CeO₂ NCs-0.5 and CeO₂ NCs-1.0), and for the higher concentration (CeO₂ NCs-2.0), it was slightly lowered compared with those of the lower concentrations, whereas in CeO₂ NCs-0.0 showing very lower values, based on these results urea playing vital role as capping and reducing agent in the formation of CeO₂ NCs.

To identify the chemical composition on the surface of the CeO₂ NCs, we performed the XPS analysis (XPS analysis only for CeO₂ NCs-0.5) and the results are presented in Fig. 4. The survey scan (Fig. S2(a)) clearly shows the presence of Ce and O elements. The high-resolution XPS spectrum of Ce shown in Fig. 4a contains six peaks, revealing that the Ce contained both the Ce³⁺ and Ce⁴⁺ oxidation states. The binding energies (BE) at 882.9, 901.2 and 917.2 eV are attributed to Ce⁴⁺, and the peaks at 885.5, 899.1 and 908.3 eV are the characteristic peaks of Ce³⁺. These results suggest the presence of mixed oxidations and a valence state for the Ce ions in the NCs^{62,63} and Deshpande⁶⁴ *et al.* reported that Ce³⁺ ions create oxygen vacancies in the CeO₂ lattice that are defects. There were three peaks in the high-resolution O 1s deconvoluted spectrum in Fig. 4b; the O1 peak, O2 peak, and O3 peak, with 529.8, 532.0, and 533.6 eV binding energies, respectively. The O1 peak (529.8 eV) corresponds to the bond Ce-O, O2 peak (532.0 eV) is attributed to the oxygen vacancies, and O3 peak (533.6 eV) belongs to organic C=O bond or surface -OH groups. To get more information we performed XPS analysis for N 1s, but the results are not showing any significant peak for N 1s and results are shown in Fig. S2(b). These results are indicating the urea was acting as capping and reduction the formation of CeO₂ NCs, not doped in CeO₂ NCs, which are similar to the values in literature^{62,65–67}.

The morphology of CeO₂ NCs was obtained by SEM, and the images are revealed in Fig. 5. For CeO₂ NCs-0.5, CeO₂ NCs-1.0, and CeO₂ NCs-2.0, SEM images show that aggregates were formed by the accumulation of nanocubes. SEM images of CeO₂ NCs-0.0 was shown in Fig. S3, the results are indicating that the CeO₂ NCs-0.0 were more in aggregation and size also higher than the urea mediated CeO₂ NCs. The details of CeO₂ NCs were further confirmed by HR-TEM studies. Fig. 6 shows the HR-TEM images of CeO₂ NCs synthesized with different concentrations of urea. The TEM images show that CeO₂ NCs were well dispersed, almost polydispersed, consisting of cubic shapes. The CeO₂ NCs obtained with 0.5 urea-based NCs were smaller in size and less aggregated

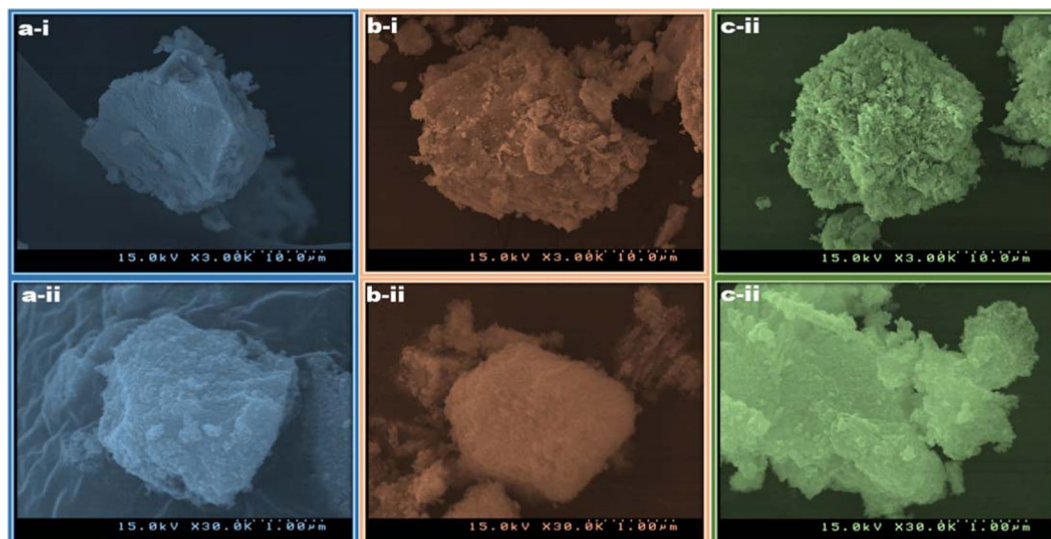


Figure 5. SEM images of the cerium oxide nanocubes as a function of urea concentrations, (a-i,ii) CeO₂ NCs-0.5, (b-i,ii) CeO₂ NCs-1.0, and (c-i,ii) CeO₂ NCs-2.0.

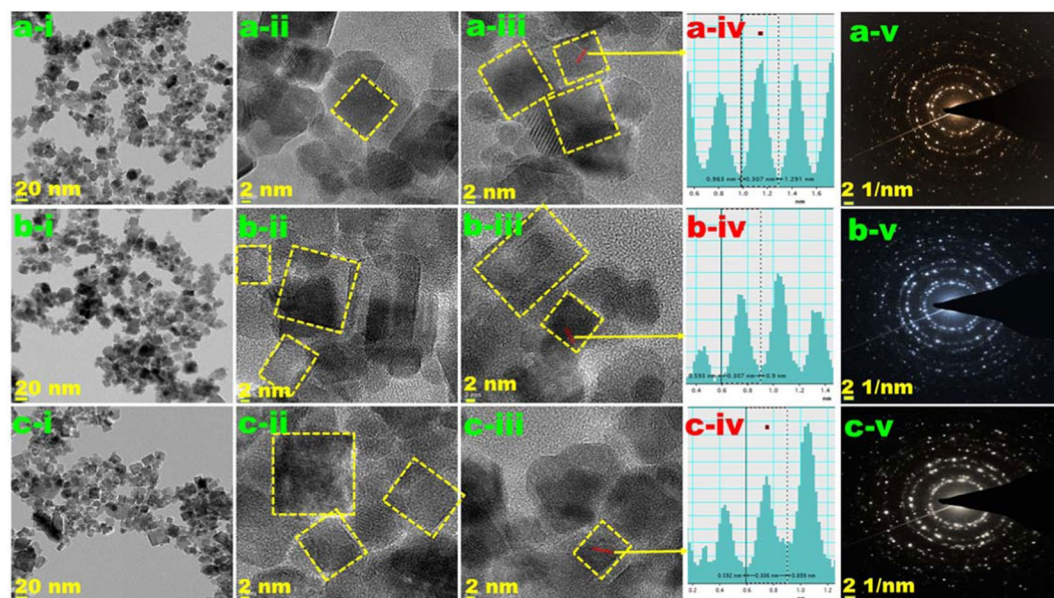


Figure 6. HR-TEM images of the cerium oxide nanocubes as a function of urea concentrations. The (a) top, (b) middle, and (c) bottom panels correspond to CeO₂ NCs-0.5, CeO₂ NCs-1.0, and CeO₂ NCs-2.0, respectively. The panels labeled i–iii show different magnifications. The respective panels labeled iv shows the *d*-spacing values and line profiles, and v correspond to the SAED patterns.

compared with the 1.0 and 2.0 urea-based NCs. To confirm the phase formation of the NCs, HR-TEM images were analyzed using the Gatan software, and the results are shown in Fig. 6a-iv–c-iv for CeO₂ NCs-0.5, CeO₂ NCs-1.0, and CeO₂ NCs-2.0, respectively. The lattice fringe distance values were similar, 0.307 nm for CeO₂ NCs-0.5, 0.307 nm for CeO₂ NCs-1.0 and 0.306 nm for CeO₂ NCs-2.0, and were assigned to the (111) plane of the CeO₂ NCs. The corresponding selected area electron diffraction (SAED) pattern (Fig. 6a-v, b-v and c-v for CeO₂ NCs-0.5, CeO₂ NCs-1.0, and CeO₂ NCs-2.0) shows well-defined diffraction rings that confirm the polycrystalline nature of CeO₂ NCs. These results were in good agreement with the XRD results. Therefore, the HR-TEM images revealed a good crystalline nature of the urea assisted NCs.

Catalytic activity. MG dye was selected as a model pollutant to examine the catalytic activity of CeO₂ NCs in the presence of NaBH₄ as the reducing agent under ambient conditions. The results are presented in Fig. 7a to c for CeO₂ NCs-0.5, CeO₂ NCs-1.0, and CeO₂ NCs-2.0, respectively. Fig. 7d shows a comparison of the absorption

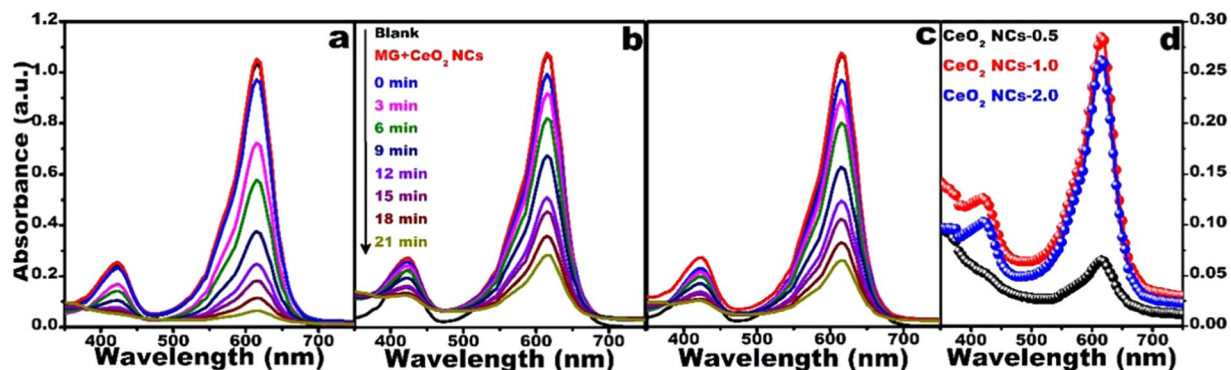


Figure 7. Time-dependent UV-visible absorption spectra of MG by NaBH_4 in the presence of (a) CeO_2 NCs-0.5, (b) CeO_2 NCs-1.0, and (c) CeO_2 NCs-2.0, and (d) comparison of catalytic activity of the samples at 21 min.

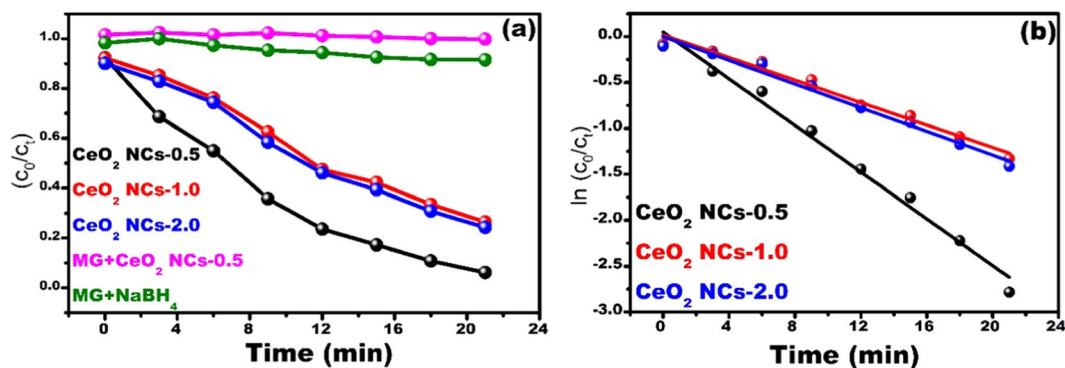


Figure 8. Catalytic activity (a), and plot of $\ln(C_0/C_t)$ (b) of CeO_2 NCs as a function of urea concentrations.

spectra of the catalytically degraded MG after 21 min in the presences of catalyst and NaBH_4 . The MG maximum absorption peak intensity was at ~ 617 nm. The intense green color of the MG dye solution slowly faded becoming colorless, during the catalytic dye degradation process. A plot of C_0/C_t versus degradation, time is shown in Fig. 8a for all samples, where C_0 is initial concentration and C_t is concentration at time 't'.

Langmuir-Hinshelwood pseudo-first order kinetics was applied to determine the first-order rate constant for dye degradation using the following relation⁶⁸:

$$k = -\ln(C_0/C_t) \quad (5)$$

where 'k' is the rate constant (min^{-1}) of the dye degradation reaction, C_0 is the initial concentration and C_t is the concentration of the dye solution after time 't' in minutes, respectively. The results are shown in Fig. 8b. To identify the role of catalyst, we performed two control experiments. In the first experiment we performed the reaction between $\text{MG} + \text{NaBH}_4 + \text{CeO}_2$ NCs and in the second experiments, we performed the reaction between dye ($\text{MG} + \text{NaBH}_4$), respectively. In both these control experiments, there was no observed degradation, based on these control experimental results we confirmed that the catalyst (CeO_2 NCs) playing a vital role in the dye decolorization, and when both the catalyst + NaBH_4 were together, the degradation materialized rapidly; the results are shown in Fig. 7a. The CeO_2 NCs-0.5 exhibited an excellent dye degradation $\sim 90\%$, while the CeO_2 NCs-1.0 and CeO_2 NCs-2.0 exhibited $\sim 70\%$ MG dye degradation within 21 min. The possible mechanism of dye reduction by the catalyst is explained by the electron relay system. The NCs start the catalytic reduction by relaying electrons from the donor BH_4^- to the dye molecules (acceptor), where the catalyst (NCs) accepted electrons from nucleophilic BH_4^- ions and transferred them to electrophilic dyes. Saikia *et al.* described hydrogen species generated from BH_4^- ions attack the dye (MG) molecules after electron transfer to nanocubes²⁶. This reaction leads to a reduction in the MG dye, which is generally leuco MG (colorless). The CeO_2 nanocatalysts show slope of -0.127 , -0.061 and -0.064 for CeO_2 NCs-0.5, CeO_2 NCs-1.0, and CeO_2 NCs-2.0, respectively. The rate constants for dye degradation were 0.127 min^{-1} , 0.061 min^{-1} , and 0.064 min^{-1} for CeO_2 NCs-0.5, CeO_2 NCs-1.0, and CeO_2 NCs-2.0, respectively (Fig. 8a,b). CeO_2 NCs-0.5 exhibited the highest dye degradation due to their size and high dispersion. We evaluated the catalytic activity of the CeO_2 NCs-0.0, the rate constant was 0.03 min^{-1} , as shown in Fig. S3 and it has shown poor performance than CeO_2 NCs-1.0 and 2.0 that of counterparts due to bigger size and aggregation of particles.

Conclusion

We developed cost-effective CeO₂ NCs using carbamide by one-pot hydrothermal method. The HR-TEM images revealed the synthesized NCs was cubic in shape. XRD results show the synthesized nanoparticles MGS of 12, 12, 13 and 31 nm for CeO₂ NCs-0.5, CeO₂ NCs-1.0, CeO₂ NCs-2.0 and CeO₂ NCs-0.0, respectively. These results were indicating that urea acting as capping and reducing agent. The synthesized CeO₂ NCs also acted as efficient catalysts in the degradation of the MG dye.

References

- Muralikrishna, I. V. & Mançikam, V. Introduction, chapter one. *Envi. Management* 1–4 (2017).
- Mondal, P., Baksi, S. & Bose, D. Study of environmental issues in textile industries and recent wastewater treatment technology. *World Sci. Reports* **61**, 98–109 (2017).
- Raval, N. P., Shah, P. U. & Shah, N. K. Malachite green a cationic dye and its removal from aqueous solution by adsorption. *Appl. Water Sci.* **7**, 3407–3445 (2017).
- Singh, A. K. & Nakate, U. N. Photocatalytic properties of microwave-synthesized TiO₂ and ZnO nanoparticles using malachite green dye. *J. Nanopart.* **2013**, 310809 (2013).
- Panandiker, A., Fernandes, C. & Rao, K. V. K. The cytotoxic properties of malachite green are associated with the increased demethylase, aryl hydrocarbon hydroxylase and lipid peroxidation in primary cultures of Syrian hamster embryo cells. *Cancer Lett.* **67**, 93–101 (1992).
- Tahir, H., Hamed, U., Sulthan, M. & Jahanzeb, Q. Batch adsorption technique for the removal of malachite green and fast green dyes by using montmorillonite clay as adsorbent. *African J. Biotechnol.* **9**, 8206–8214 (2010).
- Makeswari, M. & Santhi, T. Removal of malachite green dye from aqueous solutions onto microwave assisted zinc chloride chemical activated epicarp of *Ricinus communis*. *J. Water Resou. Prot.* **5**, 222–238 (2013).
- Al-Jawhari, I. F. H. & Al-Mansor, K. J. Biological removal of malachite green and congo red by some filamentous Fungi. *Int. J. Envi. Agri. Biotechnol.* **2**, 723–731 (2017).
- Meena, S., Vaya, D. & Das, B. K. Photocatalytic degradation of malachite green dye by modified ZnO nanomaterial. *Bull. Mater. Sci.* **39**, 1735–1743 (2016).
- Kaykhaii, M., Sasani, M. & Margzari, S. Removal of dyes from the environment by adsorption process. *Chem. Mat. Eng.* **6**, 31–35 (2018).
- Suteu, D., Bilba, D. & Coseri, S. Macroporous polymeric ion exchangers as adsorbents for the removal of cationic dye basic blue 9 from aqueous solutions. *J. Appl. Polym. Sci.* **39620** (2014).
- Manh, H. B., Ngoc, D. N. & Quoc, H. N. Effects of gamma irradiation on color removal from reactive red 24 aqueous solutions. *Sci. Technol. Develop.* **19**, 38–43 (2016).
- El Nemr, A., Hassaan, M. A. & Madkour, F. F. Advanced oxidation process (AOP) for detoxification of acid red 17 dye solution and degradation mechanism. **5**, 95–113 (2018).
- Zhu, M. X., Lee, L., Wang, H. H. & Wang, Z. Removal of an anionic dye by adsorption/precipitation processes using alkaline white mud. *J. Hazard. Mat.* **149**, 735–741 (2007).
- Soltani, T. & Entezari, M. H. Photolysis and photocatalysis of methylene blue by ferrite bismuth nanoparticles under sunlight irradiation. *J. Mol. Cat A: Chem.* **377**, 197–203 (2013).
- Moghaddam, S. S., Alavi Moghaddam, M. R. & Arami, M. Coagulation/flocculation process for dye removal using sludge from water treatment plant: Optimization through response surface methodology. *J. Hazard. Mat.* **175**, 651–657 (2010).
- Jain, R., Sharma, N. & Radhapyari, K. Electrochemical treatment of pharmaceutical azo dye amaranth from waste water. *J. Appl. Electrochem.* **39**, 577–582 (2009).
- Sripiboon, S. & Suwannahong, K. Color removal by ozonation process in biological wastewater treatment from breweries. *IOP. Conf. Series: Earth Environ. Sci.* **167**, 012010 (2018).
- De Bin, j, Xiaoying, L., Xuan, X. & Yu Xin, Z. Double-shell Fe₂O₃ hollow box-like structure for enhanced photo-Fenton degradation of malachite green dye. *J. Phys. Chem.* **112**, 209–215 (2018).
- De Bin, J. *et al.* Facile synthesis of three-dimensional/manganese silicate anorodds composites for enhanced Fenton-like catalytic dye degradation of malachite green dye. *J. Nanopart. Res.* **20**, 123 (2018).
- Wang, A. M., Qu, J. H., Liu, H. J. & Lei, P. J. Dyes wastewater treatment by reduction-oxidation process in an electrochemical reactor packed with natural manganese mineral. *J. Environ. Sci.* **18**, 17–22 (2006).
- Zuleta-Correa, A., Merino-Restrepo, A., Jimenez-Correa, S. & Hormaza-Anaguano, A. Use of white rot fungi in the degradation of an azo dye from the textile industry. *DYNA* **83**, 128–135 (2016).
- Ali Khan, K. & Srivastava, S. Decolorization and degradation of textile dyes by bacterial isolates. *Res. Environ. Life Sci.* **7**, 299–304 (2014).
- Wilfred Sugumar, R. & Sadanandhan, S. Combined anaerobic-Aerobic bacterial degradation of dyes. *E-J. Chem.* **7**, 739–744 (2010).
- Selvakumar, S., Manivasagam, R. & Chinnappan, K. Biodegradation and decolourization of textile dye wastewater using *Ganoderma lucidum*. *Biotech.* **3**, 71–79 (2013).
- Saikia, P., Miah, A. T. & Das, P. P. Highly efficient catalytic reductive degradation of various organic dyes by Au/CeO₂-TiO₂ nano-hybrid. *J. Chem. Sci.* **129**, 81–93 (2017).
- Ravishankar, T. N., Ramakrishnappa, T., Nagaraju, G. & Rajanaika, H. Synthesis and characterization of CeO₂ nanoparticles via solution combustion method for photocatalytic and antibacterial activity studies. *Chem. Open* **4**, 146–154 (2015).
- Lu, X. *et al.* Facile synthesis of free-standing CeO₂ nanorods for photoelectron chemical applications. *Chem. Comm.* **46**, 7721–7723 (2010).
- Park, S. D., Vohs, J. M. & Gorte, R. J. Direct oxidation of hydrocarbons in a solid-oxide fuel cell. *Nature* **404**, 265–267 (2000).
- Xu, C. W. & Shen, P. K. Novel Pt/CeO₂/C catalyst for electrooxidation of alcohols in alkaline media. *Chem. Comm.* **404**, 2238–2239 (2004).
- Goharshadi, E. K., Samiee, S. & Nancarrow, P. Fabrication of cerium oxide nanoparticles: Characterization and optical properties. *J. Colloid Int. Sci.* **356**, 473–480 (2011).
- Arnold, M. C., Badireedy, A. R., Wiesher, M. R., Giulia, R. T. & Meyer, J. N. Cerium oxide nanoparticles are more toxic than equimolar bulk cerium oxide in *Caenorhabditis elegans*. *Arch. Environ. Contam. Toxicol.* **65**, 224–233 (2013).
- McKerracher, R. D. *et al.* Improving the stability and discharge capacity of nanostructured Fe₂O₃/C anodes for iron-air batteries and investigation of 1-octanethiol as an electrolyte additive. *Electrochim. Acta* **318**, 625–634 (2019).
- Diego, P. *et al.* Luminescent downshifting by photo-induced sol-gel hybrid coatings: Accessing multifunctionality on flexible organic photovoltaics via ambient temperature material processing. *Adv. Electro. Mat.* **2**, 1600288 (2016).
- Beatrice, M. *et al.* One-dimensional ZnO/gold junction for simultaneous and versatile multisensing measurements. *Sci. Reports* **6**, 29763 (2016).
- Federico, B. *et al.* Combined structural, chemometric, and electrochemical investigation of vertically aligned TiO₂ nanotubes for Na-ion batteries. *ACS Omega* **3**, 8440–8450 (2018).
- Louis, L. P. *et al.* Spray-dried mesoporous mixed Cu-Ni oxide @graphene nanocomposite microspheres for high power and durable Li-ion battery anodes. *Adv. Energy Mat.* **8**, 1802438 (2018).

38. Periyat, P., Laffir, F., Tofail, S. A. M. & Magner, E. A facile aqueous sol-gel method for high surface area nanocrystalline CeO₂. *RSC Adv.* **1**, 1794–1798 (2011).
39. Tamizidurai, P. *et al.* Environmentally friendly synthesis of CeO₂ nanoparticles for the catalytic oxidation of benzyl alcohol to benzaldehyde and selective detection of nitrite. *Sci. Reports* **7**, 46372 (2017).
40. Xiong, Z. *et al.* Flame spray pyrolysis synthesized ZnO/CeO₂ nanocomposites for enhanced CO₂ photocatalytic reduction under UV-Vis light irradiation. *J. CO₂ Util.* **18**, 53–61 (2017).
41. Kumar, E., Selvarajan, P. & Muthuraj, D. Synthesis and characterization of CeO₂ nanocrystals by solvothermal route. *Mat. Res.* **16**, 269–276 (2013).
42. Bumajdad, A., Zaki, M. I., Eastoe, J. & Lata, P. Microemulsion-based synthesis of CeO₂ powders with high surface area and high-temperature stabilities. *Langmuir* **20**, 1123–1133 (2004).
43. Sharma, V., Eberhardt, K. M., Sharma, R., Adams, J. B. & Crozier, P. A. A spray drying system for synthesis of rare-earth doped cerium oxide nanoparticles. *Chem. Phys. Lett.* **495**, 280–286 (2010).
44. Tok, A. I. Y., Boey, F. Y. C., Dong, Z. & Sun, X. L. Hydrothermal synthesis of CeO₂ nano-particles. *J. Mat. Proc. Technol.* **190**, 217–222 (2007).
45. Miyazaki, H. *et al.* Synthesis of CeO₂ nanoparticles by rapid thermal decomposition using microwave heating. *Appl. Ceramics* **109**, 123–127 (2010).
46. Aneesh, P. M., Vanaja, K. A. & Jayaraj, M. K. Synthesis of ZnO nanoparticles by hydrothermal method. *Proc. Of SPIE nanophotonic Mat.* **6639**, 66390J (2007).
47. Vignesh Kumar, T. H. & Sundramoorthy, A. K. Non-enzymatic electrochemical detection of urea on silver nanoparticles anchored nitrogen-doped single-walled carbon nanotube modified electrode. *J. Electrochem. Soc.* **165**, B3006–B3016 (2018).
48. Hilding-Ohlsson, A., Fauerbach, J.A., Sacco, N.J., Bonetto, M.C. & Corton, E. Voltamperometric discrimination of urea and melamine adulterated skimmed milk powder. *Sensors (Basel)*, 12220–12234 (2012).
49. Nurhasanah, I., Safitri, W., Arifin, Z., Subagio, A. & Windarti, T. Antioxidant activity and dose enhancement factor of CeO₂ nanoparticles synthesized by precipitation method. *IOP. Conf. Series: Mat. Sci. Eng.* **432**, 012031 (2018).
50. Grdadolnik, J. & Marechal, Y. Urea and urea-water solutions-an infrared study. *J. Mol. Stru.* **615**, 177–189 (2002).
51. Valério, A., Araújo, P. H. H. & Sayer, C. Preparation of poly (urethane-urea) nanoparticles containing açai oil by miniemulsion polymerization. *Polimeros* **23**, 451–455 (2013).
52. Zamiri, R. *et al.* Dielectrical properties of CeO₂ nanoparticles at different temperatures. *Plos one* **10**, e0131851 (2015).
53. Pujar, M. S., Hunagund, S. M., Desai, V. R., Patil, S. & Sidarai, A. H. One-step synthesis and characterization of cerium oxide nanoparticles in an ambient temperature via co-precipitation method. *AIP Conf. Proc.* **1942**, 050026 (2018).
54. Chelliah, M., Rayappan, J. B. B. & Krishnan, U. M. Synthesis and characterization of cerium oxide nanoparticles by hydroxide mediated approach. *J. Appl. Sci.* **12**, 1734–1737 (2012).
55. Farahmandjou, M., Zarinkamar, M. & Firrozabadi, T. P. Synthesis of cerium oxide (CeO₂) nanoparticles using simple co-precipitation method. *Revista Mexicana de Fisica* **62**, 496–499 (2016).
56. Babitha, B. K., Sreedevi, A., Priyanka, K. P., Sabu, N. & Varghese, T. Structural characterization and optical studies of CeO₂ nanoparticles synthesized by chemical precipitation. *Indian J. Pure Appl. Phys.* **53**, 596–603 (2015).
57. Prabaharan, D. M. D. M., Sadaiyandi, K., Mahendran, M. & Sagadevan, S. Structural, optical, morphological and dielectric properties of cerium oxide nanoparticles. *Mat. Res.* **19**, 478–482 (2016).
58. Sreekanth, T. V. M. *et al.* Doo Hwan Kim, Jaesool Shim & Kisoo Yoo. Ultra-sonication-assisted silver nanoparticles using *Panax ginseng* root extract and their anti-cancer and antiviral activities. *J. Photochem. Photobiol. B: Biol.* **188**, 6–11 (2018).
59. Nagaraju, P., Vijayakumar, Y., Phase, D. M., Reddy, V. R. & Ramana Reddy, M. V. Preparation and microstructural characterization of Si(100) Ce_{1-x}Gd_xO_{2-x} thin films prepared by pulsed laser deposition technique. *Mat. Sci. Poland* **32**, 541–546 (2014).
60. Govindarajan, D. & Nithya, C. K. Structural and optical properties of cerium oxide thin films prepared by Spray Pyrolysis technique. *Int. J. Sci. Eng. Res.* **5**, 427–430 (2014).
61. Nagajyothi, P. C., Devarayapalli, K. C., Tettey, C. O., Prabhakar Vattikuti, S. V. & Jaesool, S. Eco-friendly green synthesis: catalytic activity of nickel hydroxide nanoparticles. *Mat. Res. Exp.* **6**, 055036 (2019).
62. Yeng, Y., Jin, Y., He, H. & Ye, Z. Facile synthesis and characterization of ultrathin cerium oxide nanorods. *Cryst. Eng. Comm.* **12**, 2663–2665 (2010).
63. Kar, S., Patel, C. & Santra, S. Direct room temperature synthesis of valence state engineered ultra-small ceria nanoparticles: Investigation on the role of ethylenediamine as a capping agent. *J. Phys. Chem. C* **113**, 4862–4867 (2009).
64. Deshpande, S., Patil, S., Kuchibhatla, S. & Seal, S. Size dependency variation in lattice parameter and valency states in nanocrystalline cerium oxide. *Appl. Phys. Lett.* **87**, 133113 (2005).
65. Yu, R., Yan, L., Zheng, P., Chen, J. & Xing, X. Controlled synthesis of CeO₂ flower-like and well-aligned anorods hierarchical architectures by a phosphate-assisted hydrothermal route. *J. Phys. Chem. C* **112**, 19896–19900 (2008).
66. Sreekanth, T. V. M., Nagajyothi, P. C., Dillip, G. R. & Lee, Y. R. Determination of band alignment in the synergistic catalyst of electron structure modified graphitic carbon nitride-integrated ceria-quantum dots hetero junction for rapid degradation of organic pollutants. *J. Phys. Chem. C* **121**, 25229–25242 (2017).
67. Talha, A. *et al.* I. Morphology engineering of self-assembled nanostructured CuCo₂O₄ anodes for lithium-ion batteries. *Energy Technol.* **7**, 1900295 (2019).
68. Dillip, G. R., Sreekanth, T. V. M. & Joo, S. W. Tailoring the bandgap of N-rich graphitic carbon nitride for enhanced photocatalytic activity. *Ceram. Int.* **43**, 6437–6445 (2017).

Acknowledgements

This work was supported by the National Research Foundation of Korea (NRF) grant funded by the Korean government (NRF-2017R1C1B2001990) and 2017 Yeungnam University Research Grant.

Author Contributions

The manuscript was written through the contributions of all authors. T.V.M.S.K., P.C.N.J. and G.R.R. conducted the synthesis, characterization, and application. J.S. and K.Y. designed and supervised the project.

Additional Information

Supplementary information accompanies this paper at <https://doi.org/10.1038/s41598-019-50984-6>.

Competing Interests: The authors declare no competing interests.

Publisher's note Springer Nature remains neutral with regard to jurisdictional claims in published maps and institutional affiliations.



Open Access This article is licensed under a Creative Commons Attribution 4.0 International License, which permits use, sharing, adaptation, distribution and reproduction in any medium or format, as long as you give appropriate credit to the original author(s) and the source, provide a link to the Creative Commons license, and indicate if changes were made. The images or other third party material in this article are included in the article's Creative Commons license, unless indicated otherwise in a credit line to the material. If material is not included in the article's Creative Commons license and your intended use is not permitted by statutory regulation or exceeds the permitted use, you will need to obtain permission directly from the copyright holder. To view a copy of this license, visit <http://creativecommons.org/licenses/by/4.0/>.

© The Author(s) 2019